ORIGINAL PAPER

NUMERICAL ANALYSIS OF UNSTEADY PULSATING FLOWS USING A MODIFIED WALL-FUNCTION

IONUT STELIAN GRECU[1], GEORGIANA DUNCA[1], DIANA MARIA BUCUR[1], ROBERT MITRUT[1], MICHEL CERVANTES[2]

Manuscript received: 15.09.2025; Accepted paper: 30.11.2025; Published online: 30.12.2025.

Abstract. *Nowadays, hydraulic turbines are more often operated under off-design conditions due to the increase in intermittent energy production (wind and solar). In these operating conditions, dynamic phenomena in hydraulic circuit are observed, such as flow instabilities, secondary flows, vortex rope developed in the draft tube etc. These phenomena can lead to pressure pulsations and structural vibrations of the hydraulic turbine structure, that affect the hydraulic turbine performance and its lifespan. In the present paper a wall model, developed by Manhart et al. (2008), is used with the k-ω SST turbulence model to study numerically the pulsating flows which can occur in a hydraulic turbine during part load operation. The Manhart wall model considers the adverse pressure gradient and has the advantage of being used on a coarser mesh (dimensionless distance, y^+, can result in values up to 5), leading to smaller simulation time and computational demands when compared to the general approaches. The numerical analysis is carried on using the open-source software, Code_Saturne, and considers a geometry that is similar to the draft tube of a hydraulic turbine.*

Keywords: *unsteady flows; pulsating flows; wall-function; CFD simulations.*

1. INTRODUCTION

In the last decade an increase in energy production from renewable energy sources was observed, mainly from wind and solar sources [1]. Because of their unpredictable behavior, the wind and solar are forcing the hydraulic turbines to work under off-design conditions. This can lead to part load or high load operation of hydraulic turbines which can result in the development of dynamic phenomena. The dynamic phenomena can be represented by transient flows, secondary flows, flow instability, pulsating flows etc., which can reduce the lifespan of the hydraulic turbines. Therefore, great interest from the academic and industry communities was observed on these phenomena [2-4].

To study these dynamic phenomena, experimental campaigns can be performed, but they are expensive and restrictive on the flow parameters measured. A less expensive approach is represented by performing Computational Fluid Dynamics (CFD) numerical simulations. In the last decade, high-performance computers (HPC) have become more accessible to perform numerical analyses of the flow inside the hydraulic turbines [5-8].

[1] National University of Science and Technology POLITEHNICA Bucharest, Department of Hydraulics, Hydraulic Machinery and Environmental Engineering, 060042 Bucharest, Romania. E-mail: ionut_stelian.grecu@upb.ro, georgiana.dunca@upb.ro, diana.bucur@upb.ro, robert.mitrut@upb.ro.
[2] Luleå University of Technology, Department of Engineering Sciences and Mathematics, 97187 Luleå, Sweden. E-mail: michel.cervantes@ltu.se.

https://doi.org/10.46939/J.Sci.Arts-25.4-c03

One economic approach to perform CFD numerical analyses, from the computational demand point of view, is the Reynolds Averaged Navier - Stokes (RANS) approach. Still, when complex flows are analyzed using the RANS approach challenges are encountered such as the influence of the Adverse Pressure Gradient (APG) over the flow field. The RANS approach is usually carried out using two equations turbulence models, either *k-ε* and *k-ω*, for modelling the turbulence of the flow.

To model the velocity near the wall depending on the turbulence model used different functions are involved. The Standard Wall Function (SWF) is used for the k-ε turbulence model, and the automatic wall model (AWM) is used for the k-ω turbulence model. But using these wall modelling methods leads to poor results in the case of SWF and to high computational resources demand in the case of AWM [8].

Over the last two decades, studies on wall modelling methods focused mainly on Large Eddy Simulations (LES) and Direct Numerical Simulations (DNS) [9-19]. To the authors knowledge, limited studies were performed on unsteady pulsating flows that implies the use of modified wall-functions for RANS numerical simulations. Such development is of interest to develop more efficient and accurate calculation, e.g., for optimization purposes.

This paper extends the research performed by Grecu et al. [20], by using a new set of data corresponding to another frequency for pulsating flow, 0.03 Hz. In the previous study of Grecu et al., a frequency of 0.35 Hz was considered for analysis which corresponds to a quasi-laminar regime. The quasi-laminar regime is characterized by small oscillation periods where the unsteadiness affects the flow in the near-wall region, specifically in the viscous and buffer layers. The conclusions pointed out that there was a reduction in simulation time of approximatively 50% when the Manhart wall-model was used, when compared to the standard *k-ω* SST turbulence model, while keeping the same accuracy of the results.

The value chosen for the present study also considers the flow unsteadiness, but it falls into a different pulsating flow regime known as quasi-steady regime, where the oscillation periods of the pulsating flow is larger. When the pulsating flow falls in the quasi-steady regime two regions are observed: the central region of the flow that has characteristics similar to a steady turbulent flow and the rest of the flow which is unsteady [21, 22].

The paper presents the numerical investigation of a pulsating flow with a characteristic frequency of 0.03 Hz under the influence of the APG. To analyze the pulsating flow, RANS based unsteady-state numerical simulations were performed using the *k-ω* Shear Stress Transport (SST) turbulence model.

To the *k-ω* SST turbulence model a modified wall-function developed by Manhart et al. [5] was applied. The Manhart wall-model [5] evaluates the near-wall velocity considering the influence of the streamwise pressure gradient besides the influence of the wall shear stress, as the existing classical wall-models do. The Manhart wall-model was previously validated using DNS [5] and LES [6-7].

The purpose of the present study is to evaluate alternative wall-functions that could reduce the simulation time and the computational resources demand of numerical simulations.

The Manhart wall model results were compared to the automatic wall-model from the *k-ω* SST turbulence model, and to the experimental measurements from the work of Cervantes and Engström [21]. The flow analyzed was similar to the flow inside of a hydraulic turbine draft tube characterized by an oscillating frequency of 0.03 Hz. The numerical simulations were performed with the free open-source CFD software, Code_Saturne.

2. FLOW EQUATIONS AND NUMERICAL METHOD

The analysis is performed using Unsteady Reynolds Averaged Navier - Stokes (URANS) numerical simulations. The flow equations are presented below [23,24]

$$\frac{\partial \rho}{\partial t} + \nabla\left(\rho \underline{\bar{u}}\right) = 0 \tag{1}$$

$$\frac{\partial\left(\rho \underline{\bar{u}}\right)}{\partial t} + \nabla\left(\rho \underline{\bar{u}} \otimes \underline{\bar{u}}\right) = -\nabla \bar{P} + \nabla\left[\mu\left(\nabla \underline{\bar{u}} + \nabla \underline{\bar{u}}^{T} - \frac{2}{3} tr\left(\nabla \underline{\bar{u}}\right) \underline{\underline{Id}}\right)\right] + \rho \underline{g} - \nabla\left(\rho \underline{\underline{R}}\right) + \underline{S} \tag{2}$$

where ρ, $\underline{\bar{u}}$, t, $\bar{P}$, μ, $\underline{\underline{Id}}$, $\underline{g}$, $\underline{\underline{R}}$ and $\underline{S}$ are the water density, velocity field, time, pressure field, dynamic viscosity, Kronecker delta, gravity, Reynolds's stress tensor, and other additional source terms, respectively.

Manhart [5] developed a near wall function that includes both the wall shear stress and the streamwise pressure gradient in estimating the near-wall velocity. The Manhart wall model was validated using DNS results, using a relatively coarse mesh discretization of 5 wall units, for simple cases: flow over flat plate and flow over periodic hills arrangement [5].

The streamwise pressure gradient influence is included in evaluating the velocity through a dimensionless distance, y^*, presented in equation (3).

$$y^* = \frac{y \cdot u_{\tau p}}{\nu} \tag{3}$$

where y, $u_{\tau p}$ and ν are the wall distance, characteristic velocity and kinematic viscosity, respectively.

The dimensionless distance, y^*, is based on the characteristic velocity, $u_{\tau p}$, equation (4). The characteristic velocity, $u_{\tau p}$, is determined using a velocity scale, u_τ, influenced by the wall shear stress and another velocity scale, u_p, which involves the streamwise pressure gradient. Both velocities scales are presented in equation (5).

$$u_{\tau p} = \left(u_\tau^2 + u_p^2\right)^{1/2} \tag{4}$$

$$u_\tau = \left(\frac{\tau_w}{\rho}\right)^{1/2};\ u_p = \left|\frac{\mu}{\rho^2}\frac{\partial P}{\partial x}\right|^{1/3} \tag{5}$$

To introduce the characteristic velocity in the Manhart wall model a parameter α that quantifies the influence of both streamwise pressure gradient and wall shear stress is determined, equation (6).

$$\alpha = u_\tau^2 / u_{\tau p}^2 \tag{6}$$

Therefore, the Manhart wall model takes the form presented in equation (7), in wall units.

$$u^* = sign\left(\tau_w\right)\alpha y^* + sign\left(\frac{\partial P}{\partial x}\right)\left(1-\alpha\right)^{3/2} y^{*2} \tag{7}$$

3. NUMERICAL CASE

3.1. GEOMETRY

The numerical test case considered for the numerical simulations was inspired from the experimental setup, Figure 1, of Cervantes and Engström [21]. The geometry of interest, used for the numerical simulations is marked with a discontinued red line in Figure 1.

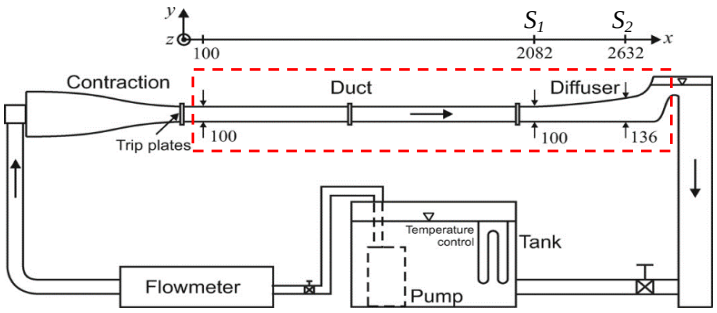

Figure 1. Experimental setup, Cervantes and Engström [8].

It contains an asymmetric diffuser preceded by a straight rectangular duct. The straight rectangular duct has a square cross section of 0.1 ×0.15 m (height x width) with a length of 2.102 m. The asymmetry of the diffuser is represented by the diverging upper wall, starting with an angle of 2.5° and it gradually increasing to 7.5° until the diffuser outlet.

The available experimental data used in the validation of the numerical analyses consists of velocity measurements presented in [21]. The velocity data were measured very close to the wall, up to $y^+ = 1$, using laser Doppler anemometry (LDA) technique in two sections of the diffuser, at its half width. The first section, S_1, was located near the beginning of the diffuser and the second section, S_2, was located near the diffuser elbow. The flow rate was set to $2.47 \cdot 10^{-3}$ m^3/s, and the pulsations of the flows were generated by controlling the electric current frequency of the pump resulting in oscillations with the frequency of 0.03 Hz. In the present study the same frequency is analyzed.

3.2. NUMERICAL SETUP

To assess the Manhart wall model performance, the numerical simulations results are compared with the standard wall model from the k-ω SST turbulence model and the experimental measurements from the work of Cervantes and Engström [21]. The comparison is carried out in terms of computational resources (time and power) when compared with the standard k-ω SST turbulence model and in terms of precision when compared to the experimental data.

To generate the optimum mesh for each wall model and to properly represent the behavior of the pulsating flows, mesh and time-step sensitivity studies were performed. The sensitivity studies were based on the Stokes second problem [25] case and the Nyquist-Shannon theorem. Therefore, generating an optimum mesh for the pulsating flow analysis required at least 50 uniform cell layers in the oscillating layer. Also, to resolve the pulsating flows oscillations, a time-step which leads to a maximum Courant number of 50 and at least 40 data points over one oscillation was required.

The meshes used for each wall model were generated using the ICEM CFD, with different refinement of the near-wall zone, y^+, as presented in Table 1, along with other mesh

properties. The meshes were generated using hexahedral cells while respecting the mesh quality criteria required by Code_Saturne. The time-step of the numerical simulations was set to 0.01 s to respect the Courant number condition.

Table 1. Mesh properties.

Numerical simulation	Mesh req. for y^+	Averaged y^+	Mesh size [10^6 cells]
k-ω SST	≈ 1	0.34	11 800
Manhart k-ω SST	≤ 5	0.86	5 317

The boundary conditions, presented in Figure 2, were defined to best resemble the experimental procedure [21]. The inlet boundary condition was defined to follow a cosine function, equation (8), to generate oscillations with a frequency of 0.03 Hz. The outlet boundary condition was set to a relative pressure of 0 Pa. The no-slip condition with zero roughness was applied for the walls.

$$u_{in} = 0.165 \cdot \left(1 + \left(A_{Uc} / U_c\right) \cdot \cos\left(2\pi f \cdot t\right)\right) \tag{8}$$

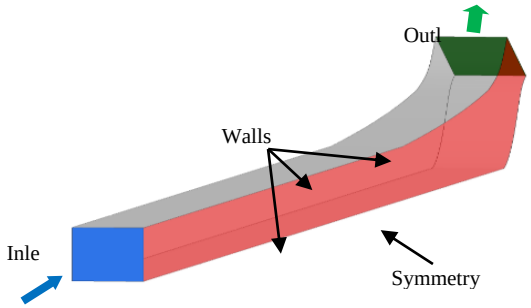

Figure 2. Boundary conditions numerical test case.

The unsteady numerical simulations were carried out using the SIMPLEC algorithm of the segregated double precision solver of Code_Saturne. The Second Order Linear Upwind scheme (SOLU) for the convective scheme of the solver was used. The time dependent term was calculated using an implicit first order Euler θ-scheme. The numeric method was defined using the Jacobi method for velocity field, turbulent kinetic energy and specific rate of dissipation, and Conjugate Gradient method for pressure. Also, the gradient of the flow variables was computed using a least-square method with a standard evaluation of neighborhood cells. The considered convergence criteria were the flow variables residuals, where a precision of 10^{-6} was achieved, and the periodic state of several streamwise velocity monitor points placed near the bottom wall of the diffuser [24].

4. NUMERICAL RESULTS

The Manhart wall model was evaluated by comparing the numerical results to the standard k-ω SST turbulence model results and to the experimental data in the two sections, S_1 and S_2. The first section was located 20 mm before the diffuser inlet, where a negative pressure gradient affects the flow, and the second section was located near the diffuser elbow where an adverse pressure gradient is affecting the flow. The flow variables evaluated in the comparisons are time-averaged variables: wall shear stress, τ_w, friction velocity, u_τ, dimensionless streamwise velocity, U^+, and dimensionless turbulence production, P_k^+.

The wall shear stress, τ_w, and the friction velocity, u_τ, determined using the polynomial approximation from [21] are presented in Table 2, alongside the experimental values to assess the wall models precision.

Table 2. Time-averaged flow variables.

Test case conditions	Wall shear stress, τ_w		Friction velocity, u_τ	
	Section S_1	Section S_2	Section S_1	Section S_2
Experiment data	0.09	0.045	0.0095	0.0067
k-ω SST	0.067	0.033	0.0082	0.0057
Manhart k-ω SST	0.064	0.030	0.0080	0.0055

Both wall models underestimate the values of the wall shear stress and the friction velocity when compared with the experimental data. A possible cause for the underestimated values could be from the numerical test case. In the experimental procedure the boundary layer was tripped close to the duct inlet leading to secondary flow which were not considered in defining the settings of the inlet boundary condition of the numerical simulations.

The dimensionless streamwise velocity, U^+, was calculated using equation (9).

$$U^+ = \frac{\overline{u}}{u_\tau} \tag{9}$$

In Figure 3 the variation of the streamwise velocity, U^+, is presented against the dimensionless distance y^+. Both variables were normalized using their maximum value for both sections.

When compared to the standard k-ω SST results the Manhart wall model returns a good estimation of the velocity profiles over the entire spectrum of data. When compared to the experimental data all wall models are slightly deviated when reaching the buffer layer, where $y^+ = 0.02$, because of the underestimation of the wall shear stress.

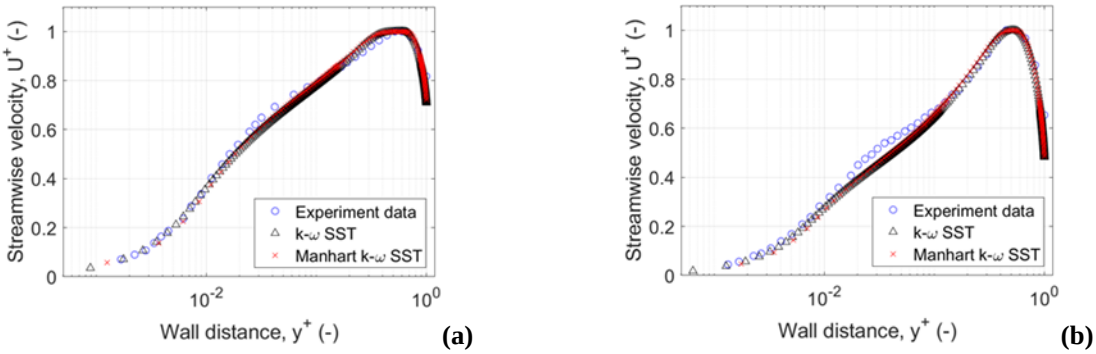

Figure 3. Time-averaged streamwise velocity distribution: (a) section S_1 and (b) section S_2.

In Figure 4 the turbulence production profiles are presented in both sections, calculated using equation (10). Also, in Figure 4 the variables are normalized using their maximum value for each section.

$$P_k^+ = \left(\mu_t \left(\frac{\partial u_i}{\partial x_j} + \frac{\partial u_j}{\partial x_i} \right) \frac{\partial u_i}{\partial x_j} - \frac{2}{3} \rho k \frac{\partial u_k}{\partial x_k} \right) \cdot \left(\frac{u_\tau^3}{\delta_{99}} \right)^{-1} \tag{10}$$

where μ_τ is the turbulent viscosity, δ_{99} is the thickness of the boundary layer, and i, j, k are the velocity components indices.

It can be seen that all wall models underestimate the experimental data in both sections, presenting a small deviation of the data. Still, the wall models are following the experimental data variation and also show a good estimation of the position of the turbulence production maximum value.

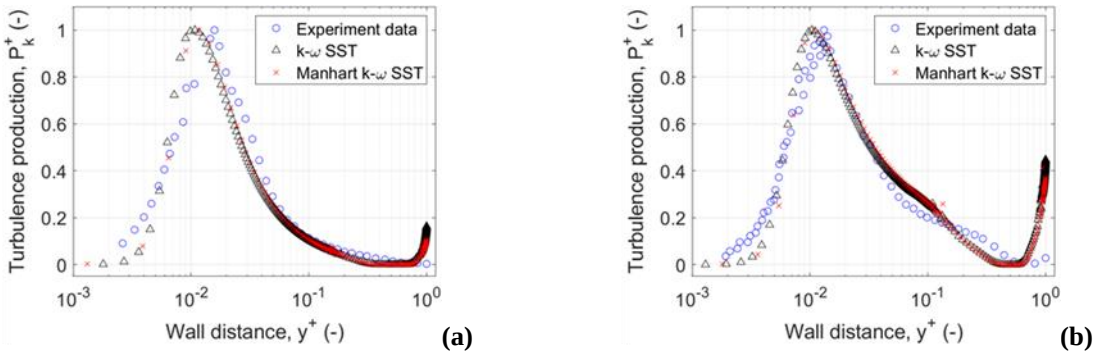

Figure 4. Dimensionless turbulent production variations: (a) section S_1 and (b) section S_2.

The simulation performed with the standard *k-ω* SST wall model completed in approximately 600 hours while the simulation performed with the Manhart Wall model completed in 127 hours. Therefore, the Manhart wall model showed a reduction in simulation time compared to the standard *k-ω* SST of 78.8%. To be noted that all the numerical simulations were performed on the same workstation.

4. CONCLUSIONS

The paper presents the numerical investigation of a pulsating flow based on a frequency which corresponds to a quasi-steady regime. The paper extends the research performed by Grecu et al. [20], by using a new set of data corresponding to another frequency for pulsating flow, 0.03 Hz. The 0.03 Hz frequency corresponds to a quasi-steady regime with large oscillation periods, the regime shows similarities to a steady turbulent flow at each instant of time except in the near-wall region where the flow is affected by unsteadiness.

The research considers a modified wall-function developed by Manhart that evaluates the near-wall velocity using CFD numerical analysis. The Manhart wall-model considers the streamwise pressure gradient in the evaluation of the near-wall velocity besides the wall shear stress, as the existing classical wall-models do.

The numerical simulations presented in this paper are based on the RANS approach and the *k-ω* SST turbulence model. The results of the Manhart wall-model were compared with the standard *k-ω* SST wall-model, for economic reasons, and with experimental data, for validation.

The comparisons of the Manhart wall-model show a good approximation of the standard *k-ω* SST wall-model over the entire set of data, from the wall to the center of the diffuser, in both sections. The advantage of the Manhart wall-model can be quantified in the reduction of the simulation time, with almost 80 % less time required for achieving the same results. When compared with the experimental data, both wall-models underestimate the dimensionless velocity in the buffer layer in both sections. A cause of the underestimation might be the evaluation of the friction velocity. The turbulent production is also underestimated on approximately the entire set of data, when the wall-models results are compared to experimental data. The comparison between experiment and numerical simulations shows a match at the maximum value of turbulent production.

Therefore, as observed, for faster numerical simulation results the Manhart wall-model can be considered as an alternative to the standard *k-ω* SST wall model, due to using a coarser mesh, until $y^+ = 5$.

Further research could investigate how the Manhart wall model evaluates the velocity near the wall if the tripping of the boundary layer is included in the numerical simulations, as the experimental procedure was carried out.

To evaluate the Manhart wall model potential other investigations could be performed: using a coarser mesh for the asymmetric diffuser or using other geometries as a full draft tube hydraulic turbine.

REFERENCES

[1] IEA 2022 Energy Statistics Data Browser – Data Tools IEA.
[2] Kumar, S., Cervantes, M. J., Gandhi, B. K., *Renewable and Sustainable Energy Reviews*, **136**, 2021.
[3] Keck, H., Sick, M., *Acta Mechanica*, **201**, 211, 2008.
[4] Kundu, P. K., Cohen, I. M., Dowling, D. R., *Fluid mechanics*, Academic Press, Waltham, 2012.
[5] Manhart, M., Peller, N., Brun, C., *Theoretical and Computational Fluid Dynamics*, **22**, 243, 2008.
[6] Duprat, C., *Simulation numérique instationnaire des écoulements turbulent dans les diffuseur de centrales hydrauliques en vue de l'amélioration des performances - PhD Thesis*, Institut National Polytechnique de Grenoble – INPG, Grenoble, 198, 2010.
[7] Duprat, C., Balarac, G., Métais, O., Congedo, P.M., Brugière, O., *Physics of Fluids*, **23**, 015101, 2011.
[8] Vittori, G., Blondeaux, P., Mazzuoli, M., *Journal of Marine Science and Engineering*, **8**, 893, 2020.
[9] Xue, K., Quosdorf, D., Zhao, L., Manhart, M., *Physics of Fluids*, **36**, 075106, 2024.
[10] Bose, S., & Park, G.I., *Annual review of fluid mechanics*, **50**, 535, 2018.
[11] Cheng, W., Pullin, D. I., Samtaney, R., *Journal of Fluid Mechanics*, **785**, 78, 2014.
[12] Larsson, J., Kawai, S., Bodart, J. A., Bermejo-Moreno, I., *Mechanical Engineering Reviews*, **3**(15), 00418, 2016.
[13] Bae, H. J., Lozano-Durán, A., Bose, S., Moin, P., *Journal of Fluid Mechanics*, **859**, 400, 2018.
[14] Mukha, T., Rezaeiravesh, S., Liefvendahl, M., *Computer Physics Communications*, **239**, 204, 2018.
[15] Gao, W., Cheng, W., Samtaney, R., *Journal of Fluid Mechanics*, **900**, A43, 2020.
[16] Kawai, S., Larsson, J., *Physics of Fluids*, **25**, 015105, 2013.
[17] Gungor, A. G., Maciel, Y., Simens, M. P., Soria, J., *International Journal of Heat and Fluid Flow*, **59**, 109, 2016.
[18] Chen, Z., Hickel, S., Devesa, A., Berland, J., Adams, N. A., *Theoretical and Computational Fluid Dynamics*, **28**, 1, 2014.
[19] Bose, S., Moin, P., *Physics of Fluids*, **26**, 015104, 2014.
[20] Grecu, I. S., Dunca, G., Bucur, D. M., Cervantes, M. J., *IOP Conf. Ser.: Earth Environ. Sci.*, **1079**, 012087, 2022.
[21] Cervantes, M. J., Engström, T. F., *Journal of Hydraulic Research*, **46**, 112, 2008.
[22] Sundstrom, L. R. J., Mulu, B. G., Cervantes, M. J., *Journal of Fluid Mechanics*, **788**, 521, 2016.
[23] Pope, S., *Turbulent Flows*., Cambridge University Press., Cambridge, 2000.
[24] Électricité de France, *Code Saturne Theory Guide*, Électricité de France R&D, Paris, 2018.
[25] Schlichting, H., Gersten, K., *Boundary-Layer Theory*, Springer, Berlin Heidelberg, 2017.